Local wind speed forecasting based on WRF-HDWind coupling

D. Prieto-Herráez [a, *], L. Frías-Paredes [b, *], J.M. Cascón [c, e], S. Lagüela-López [a], M. Gastón-Romeo [b],
M.I. Asensio-Sevilla [d, e], I. Martín-Nieto [a], P.M. Fernandes-Correia [b], P. Laiz-Alonso [d], O.F. Carrasco-Díaz [f],
C. Sáez-Blázquez [a], E. Hernández [g], L. Ferragut-Canals [d, e], D. González-Aguilera [a]

[a] Cartographic and Land Engineering Department, University of Salamanca, EPS Ávila, Calle Hornos Caleros 50, 05003 Ávila, Spain
[b] CENER (Nacional Renewable Energy Centre), Ciudad de la Innovación 7, 31621 Sarriguren, Navarre, Spain
[c] Economy and Economic History Department, University of Salamanca, Building FES, Campus Miguel de Unamuno, 37007 Salamanca, Spain
[d] Applied Mathematics Department, University of Salamanca, Casas del Parque 2, 37008 Salamanca, Spain
[e] Fundamental Physics and Mathematics University Institute, University of Salamanca, Casas del Parque 1, 37008 Salamanca, Spain
[f] MatCom, San Fernando 4542, Santiago, Chile
[g] Mathematics Department, Federico Santa Maria's University, Avenida España 1680, Valparaíso, Chile

ARTICLE INFO

ABSTRACT

Wind speed forecasts obtained by Numerical Weather Prediction models are limited for fine interpretation in heterogeneous terrain, in which different roughnesses and orographies occur. This limitation is derived from the use of low-resolution and grid-box averaged data. In this paper a dynamical downscaling method is presented to increase the local accuracy of wind speed forecasts. The proposed method divides the wind speed forecasting into two steps. In the first one, the mesoscale model WRF (*Weather Research and Forecasting*) is used for getting wind speed forecasts at specific points of the study domain. On a second stage, these values are used for feeding the HDWind microscale model. HDWind is a local model that provides both a high-resolution wind field that covers the entire study domain and values of wind speed and direction at very located points. As an example of use of the proposed method, we calculate a high-resolution wind field in an urban-interface area from Badajoz, a South-West Spanish city located near the Portugal border. The results obtained are compared with the values read by a weathervane tower of the *Spanish State Meteorological Agency* (AEMET) in order to prove that the microscale model improves the forecasts obtained by the mesoscale model.

1. Introduction

The near-surface wind speed has a considerable importance in our society (e.g., insurance industry, coastal erosion, forest and infrastructure damage, storm surges, air-sea exchange). They have significant relevance in applications such as pollutant diffusion evaluation, forest fires modelling, construction issues or even wind energy resource estimation. Moreover, surface wind speeds exhibit variability at much smaller spatial scales than that resolved by mesoscale Numerical Weather Prediction (NWP) models. Hence there is a need to develop tools for downscaling NWP to generate finer scale projections of near-surface wind climatologies (Salameh et al., 2009).

The prediction of the meteorological variable corresponding to the wind can be made at different scales (Sánchez et al., 2013), being the most widely used two of the scales defined by Orlanski (1975): mesoscale (up to 2 km) and microscale (less than 2 km). The wind predictions calculated by mesoscale models usually have low spatial resolution. This limitation makes difficult its application to heterogeneous areas providing results that do not reflect local characteristics, such as topography or roughness (El-Samra et al., 2018; Fernández-González et al., 2018; Hari-Prasad et al., 2017; Trapero et al., 2013; Wagenbrenner et al., 2016). These and other local features may be incorporated into the weather forecast through the use of microscale models.

However, the use of microscale models is not enough by itself. The weather is the result of the interaction of different factors be-

* Corresponding authors.
Email addresses: dpriher@usal.es (D. Prieto-Herráez); lfrias@cener.com (L. Frías-Paredes)
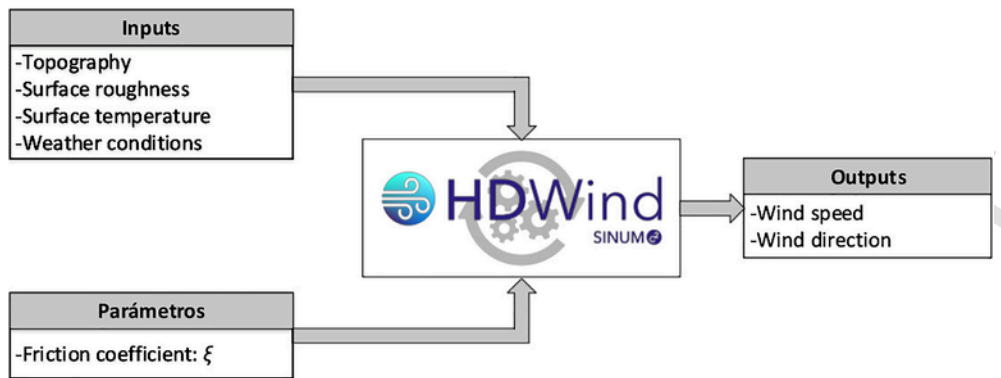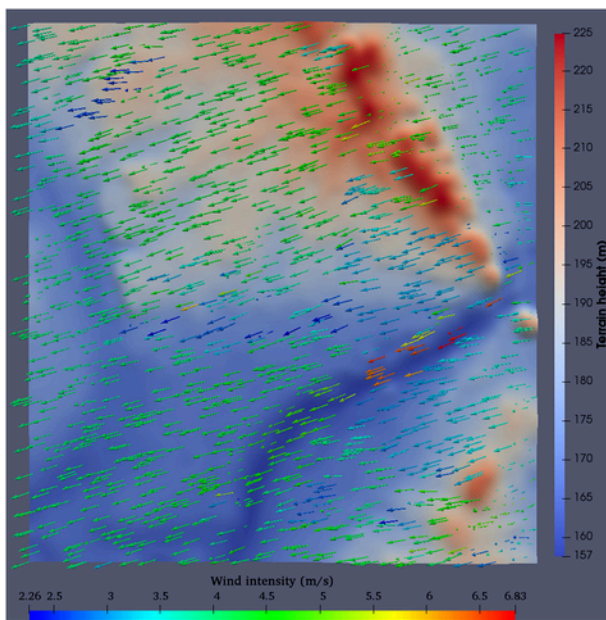
Fig. 1. HDWind input and output scheme.

Fig. 2. Simulated high-resolution wind field at 10 *m* with HDWind.

Fig. 3. WRF domains used to obtain the wind forecast.

Table 1
Physics schemes used in the WRF model setup.

WRF version	3.8.1 (modified)
Grid	2 nests: 9 *km*, 3 *km*; 35 vertical levels, 1-way nesting
Land use data	Corine 100 *m* (2012)
Land Surface Model	NOAH-LSM (Tewari et al., 2004)
height 1 pt. Planetary Boundary Layer	MYNN 2.5 level TKE scheme (Nakanishi and Niino, 2009)
Surface Layer	MYNN 2.5 level TKE scheme (Nakanishi and Niino, 2009)
Microphysics	WRF Single-Moment 5-class scheme (WSM) (Hong et al., 2004)
Long Wave Radiation	RRTMG scheme (Iacono et al., 2008)
Short Wave Radiation	RRTMG scheme (Iacono et al., 2008)
Cumulus Parameterisation	Kain-Fritsch scheme (Kain, 2004) (only used in the outermost domain (9 *km* resolution))

Currently, some authors propose the coupling of mesoscale and microscale models for wind speed forecasting (see references below). In this way, usually known as downscaling, the microscale models adapt the predictive information provided by the mesoscale models to local characteristics. There are mainly two ways to make this approach according to the nature of the local adjustment: dynamical downscaling and statistical downscaling. Dynamical downscaling is well established and widely used (Gopalan et al., 2014; Mughal et al., 2018; Oliver et al., 2015; Sanz-Rodrigo et al., 2017; Tominaga et al., 2011; Verkaik et al., 2006; Wagenbrenner et al., 2016; Yamada and Koike, 2011). It is a general method which can be applied anywhere over the globe (Xue et al., 2014), but the amount of time and resources needed to carry out the simulation can be a challenge whenever a real-time assessment is required. In order to overcome this limitation of dynamic downscaling, some authors propose a statistical downscaling (Liu and Ren, 2015; Manor and Berkovic, 2015; Otero-Casal et al., 2019; Sunyer et al., 2012) as an alternative that allows the adjustment to the peculiarities of the terrain in real-time applications.

The deep knowledge about the behavior of prediction errors is also an issue worthy of being investigated. There are recent works focused on identifying the characteristics of deviations, as the temporal point of view compiled by the Temporal Distortion Index (TDI) and Dynamic Mean Absolute Error (DMAE) proposed by Frías-Paredes et al. (2016, 2018), and its application to improve the management of wind energy generation (Frías-Paredes et al., 2017).

In this paper we continue the trend based on the mesoscale-microscale coupling strategy to improve the estimation of wind pre-

sides the local characteristics: the shape of our planet, its rotation and translation, the inclination of the axis of rotation, distance and trajectory with the sun, quantity and distribution of land and sea, sea currents, etc. Through the use of microscale models, it is not possible to contemplate all these phenomena, so its temporal scope is limited.
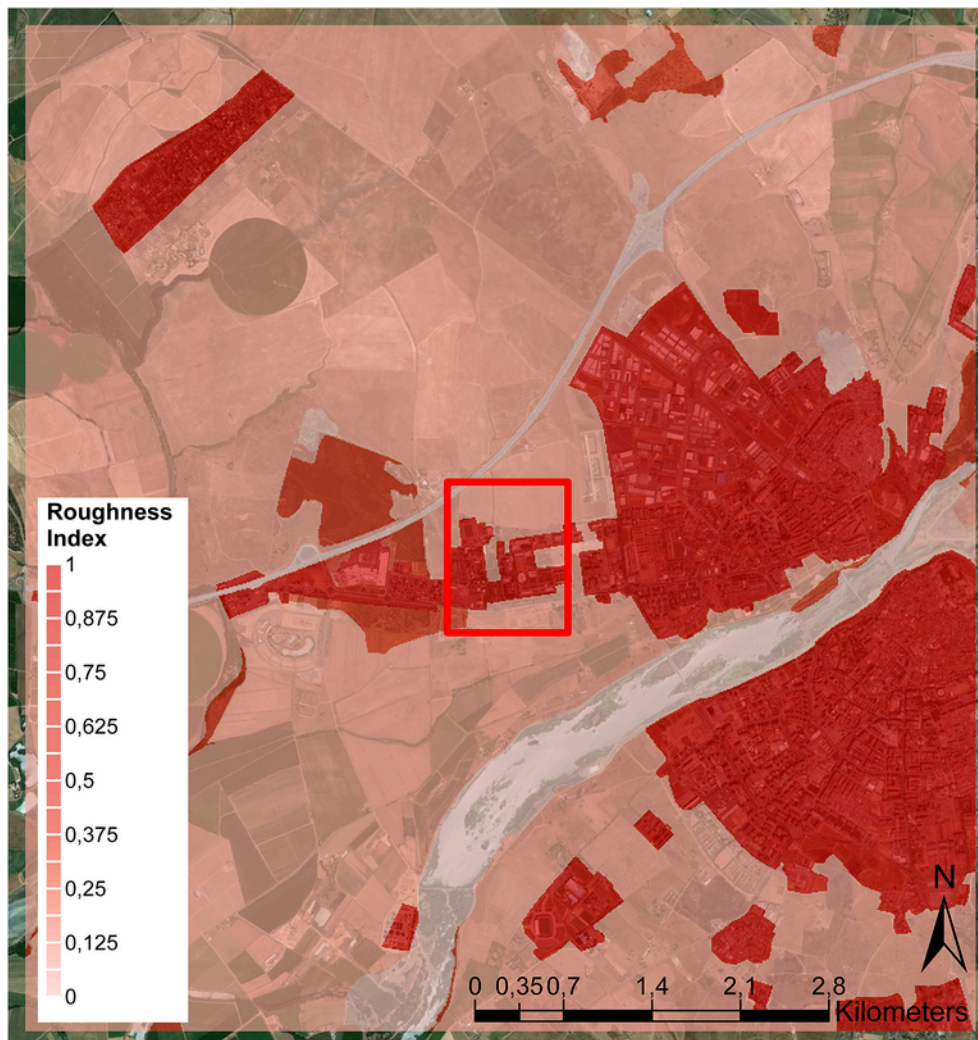
Fig. 4. Roughness index of the HDWind simulation area. The red squared indicates where the WRF output and weather station are located (see Fig. 5).

diction at the local scale. Specifically, we perform a dynamic down-scaling using the output of the *Weather Research and Forecasting* (WRF) mesoscale prediction model as input data for the HDWind microscale model. Thanks to the use of advanced numerical techniques, it is possible to perform the simulation in the local domain in a reasonable period of time. Specifically, the computational cost of the simulation involving a period of 423 days for the study domain (see Section 2.2) was about 1.269 h for the WRF simulation (3 h per simulated day) and 20 min for the HDWind simulation.

The WRF model (Skamarock et al., 2008) is one of the most used mesoscale models both in research and operational frameworks. It is an NWP model appropriated for a wide range of applications including real-time predictions, data assimilation development and studies, atmospheric parameterized-physics research, regional climate simulations, air quality modelling, atmosphere-ocean coupling, idealized simulations, etc. There are other mesoscale models but their use is not available to the public, like HIRLAM.[1]

The HDWind model (Ferragut et al., 2011), developed by the Research Group on *Numerical Simulation and Scientific Calculus* (SINUMCC) of the *University of Salamanca* to which most of the authors belong, provides a high-resolution wind field that adjusts spe-

cific wind measurements to the local characteristics, such as the slope, the roughness of the terrain or the gradients of temperature on the surface.

This paper is organized according to the following structure. Section 2 briefly reviews the two models used for the accurate wind speed estimation and their configuration: WRF (in Section 2.1.1) for generating the long-term prediction and HDWind (in Section 2.1.2) for its local adjustment. Section 2.1.3 explains the procedure followed for the coupling of the two models. The simulation scenario is described in detail in Section 2.2, where the configuration details used for the WRF (in Section 2.2.1) and HDWind (in Section 2.2.2) models is also collected. In section 3, the proposed procedure is applied to evaluate the improvement obtained through the dynamic downscaling, and the simulation results are analyzed. Finally, the paper ends with its conclusions in Section 4.

2. Experimental design

2.1. Numerical weather prediction models

2.1.1. Mesoscale model: weather research and forecasting

The WRF model is a NWP and atmospheric simulation system developed by multiple agencies -the *National Center for Atmospheric Research* (NCAR), the *National Oceanic and Atmospheric Adminis-*

---

[1] http://hirlam.org/

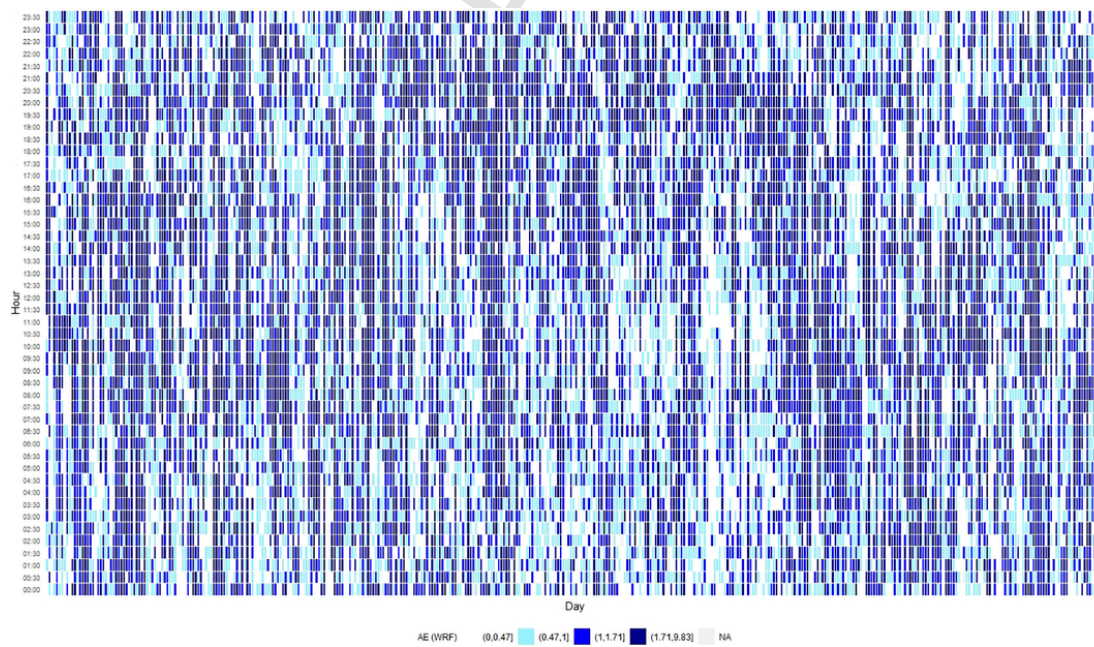**Fig. 5.** Location of WRF output and weather station.

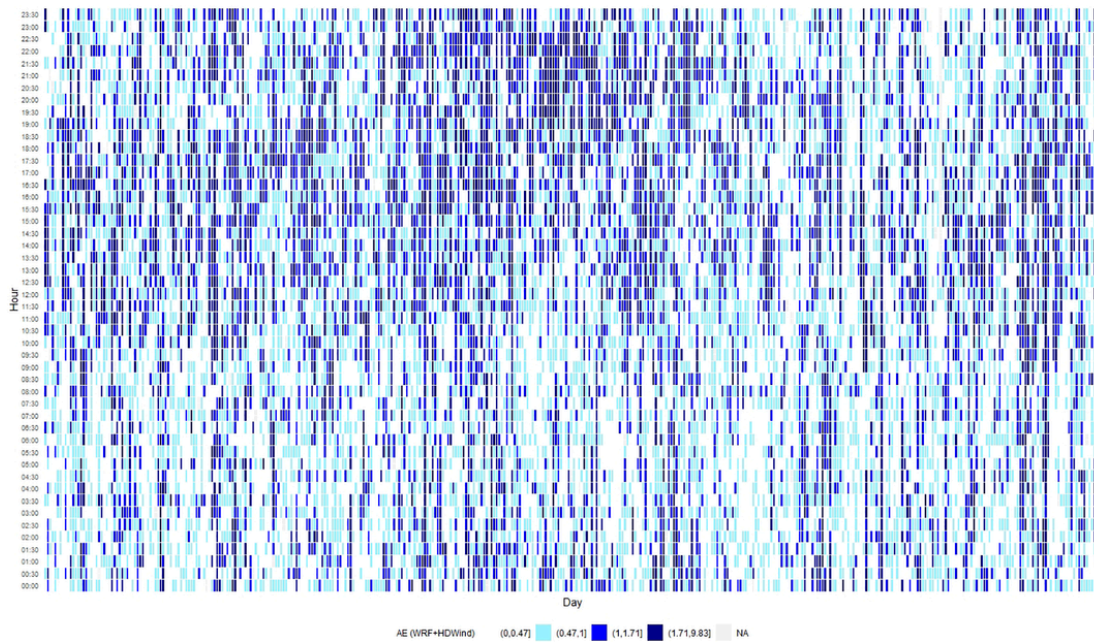**Fig. 6.** Absolute error presented by the WRF simulation.

Fig. 7. Absolute error presented by the WRF + HDWind simulation.

tration (NOAA), the *Air Force Weather Agency* (AFWA), the *Naval Research Laboratory* (NRL), the *Center for Analysis and Prediction of Storms* (CAPS) and the *Federal Aviation Administration* (FAA)-. This model was chosen for the development of this work because it is considered as one of the most advanced state-of-the-art NWP systems (Michalakes et al., 2001) and it has been widely and thoroughly validated. It is used in a regular basis by the scientific and wind energy community both for operational real-time forecasts and long-term simulations.

WRF is a robust and versatile model, capable of handling several sources of static and dynamic data and can be used with relatively confidence in a wide range of terrains, locations and meteorological regimens. This model has been designed to be a framework for NWP models developed by a multi-agency collaboration project. It is a modular single-source code that can be configured to serve both for operational forecasting and for atmospheric research (Skamarock et al., 2008). It is also a supported "community model", a free and shared resource with distributed development and centralized support. Besides, WRF is open source and its use does not require any license.

WRF has two dynamical cores: the *Advanced Research WRF* (ARW) and the *Nonhydrostatic Mesoscale Model* (NMM). The ARW core development and support are centered at the *Mesoscale & Microscale Meteorology* (MMM) department of NCAR, while the NMM core development is centered at the *Environmental Modelling Center* (EMC) of NOAA and the support is provided by the *Developmental Testbed Center* (DTC) department in NCAR.

The ARW dynamical core has been used in this work. The dynamical core is fully compressible, based on Euler primitive equations in non-hydrostatic conservative formulation but with hydrostatic option (Ooyama, 1990). It includes solvers with a large suite of options for numerical schemes and parameterization of physical processes. In its primitive equation systems, it incorporates advection, pressure gradients, Coriolis, buoyancy, filters, diffusion and time-stepping. The basic prognostic variables are the velocity components, the air potential temperature, the mixing ratios of hydrometeors and the perturbations from a hydrostatic reference state of the geopotential and surface pressure of dry air. The vertical levels are based on mass terrain-following hydrostatic pres-

sure vertical coordinates (sigma) (Laprise, 1992) and the top of the model is a constant pressure surface (Skamarock et al., 2008).

The WRF-ARW horizontal grid is the Arakawa C-grid staggered (Arakawa and Konor, 1996). The advection is solved by 2nd, 3rd, 4th, 5th and 6th order centered and upwind biased schemes. In the temporal dimension, the model uses a time-split integration using a 2nd or 3rd-order Runge-Kutta scheme with adaptive time step option (Klemp et al., 2007).

2.1.2. Microscale model: HDWind

The origin of the high-resolution wind field model HDWind lies in an asymptotic approximation of the primitive Navier-Stokes equations on the assumption that the horizontal dimensions of the simulation domain are much larger than the vertical dimension, resulting in a mass consistent vertical diffusion model capable of providing a 3D wind field by solving only 2D linear equations. The model includes other simplifications: the nonlinear terms of the Navier-Stokes equations are neglected, it is assumed that the air temperature decreases linearly with altitude and the air compressibility is neglected. The details of how the HDWind model equations are derived can be found in (Asensio et al., 2005).

The 2D equations involved in the model depend on the orography and the temperature on the ground surface, which allows to reflect the local effects due to the orography and the surface temperature gradients. The model also depends on the horizontal components of the wind at the boundary of the domain. The model depends on a single parameter, the inverse of the friction coefficient $\xi = \frac{1}{\zeta}$, which is defined in terms of the roughness length of the terrain z_0 (see Ferragut et al. (2011)). These equations provide a high-resolution 3D wind field in an air layer over the study surface, above which the orography and the temperature of the surface have no influence.

In Ferragut et al. (2011), the wind field provided by HDWind is fitted to specific wind measurements v_i, $i = 1, \ldots, n$ located at several points $P_i = (x_i, y_i, z_i)$, $i = 1, \ldots, n$ within the 3D domain. This adjustment requires the resolution of an optimal control problem in which the airflow at the horizontal domain boundary is the control element. In this way, the model does not require the measure-

Table 2
AE of the WRF simulation and of the WRF + HDWind simulation using different microphysics parameterizations.

Microphysics	Ferrier		Godddard		Kessler		Lin		Morrison		Thomson		WSM3		WSM5		WSM6	
Date	WRF	WRF + HDWind	WRF	WRF + HDWind	WRF	WRF + HDWind	WRF	WRF + HDWind	WRF	WRF + HDWind	WRF	WRF + HDWind	WRF	WRF + HDWind	WRF	WRF + HDWind	WRF	WRF + HDWind
15/03/2017	77.07	44.93	81.66	45.46	75.86	47.65	85.90	47.12	93.33	46.67	82.37	44.56	75.92	46.90	84.62	33.84	86.52	42.69
11/05/2017	168.40	40.32	162.89	40.54	176.89	41.71	163.61	39.68	166.61	40.47	165.10	39.23	166.96	41.32	150.93	36.43	162.63	40.26
12/05/2017	139.97	39.57	133.65	34.26	142.55	40.95	137.82	37.26	137.74	36.25	133.37	33.65	137.98	39.71	125.65	43.20	129.46	35.24
13/05/2017	76.88	23.97	67.56	22.63	77.87	23.85	71.48	22.83	67.82	22.49	65.41	23.74	74.61	23.17	62.00	20.74	68.82	21.10
26/06/2017	75.46	45.18	73.45	46.36	76.43	45.82	74.05	46.06	73.92	46.18	73.88	46.14	76.93	45.53	78.12	37.61	71.29	46.96
11/12/2017	121.54	60.04	129.96	51.72	126.71	49.36	136.53	48.30	129.94	50.88	125.06	52.24	127.40	54.46	120.01	36.06	137.34	48.06
Average	109.88	42.34	108.19	40.16	112.72	41.56	111.57	40.21	111.56	40.49	107.53	39.93	109.97	41.85	103.56	34.65	109.34	39.05
Total	659.30	254.01	649.17	240.97	676.30	249.34	669.40	241.25	669.37	242.94	645.18	239.56	659.79	251.09	621.33	207.88	656.06	234.31

Table 3
MAE of the WRF simulation and of the WRF + HDWind simulation using different microphysics parameterizations.

Microphysics	Ferrier		Godddard		Kessler		Lin		Morrison		Thomson		WSM3		WSM5		WSM6		WDM5	
Date	WRF	WRF + HDWind	WRF	WRF + HDWind	WRF	WRF + HDWind	WRF	WRF + HDWind	WRF	WRF + HDWind	WRF	WRF + HDWind	WRF	WRF + HDWind	WRF	WRF + HDWind	WRF	WRF + HDWind	WRF	WRF + HDWind
15/03/2017	1.64	0.96	1.74	0.97	1.61	1.01	1.83	1.00	1.99	0.99	1.75	0.95	1.62	1.00	1.80	0.72	1.84	0.91	1.86	0.90
11/05/2017	3.58	0.86	3.47	0.86	3.76	0.89	3.48	0.84	3.54	0.86	3.51	0.83	3.55	0.88	3.21	0.78	3.46	0.86	3.48	0.85
12/05/2017	2.98	0.84	2.84	0.73	3.03	0.87	2.93	0.79	2.93	0.77	2.84	0.72	2.94	0.84	2.67	0.92	2.75	0.75	2.77	0.76
13/05/2017	1.64	0.51	1.44	0.48	1.66	0.51	1.52	0.49	1.44	0.48	1.39	0.51	1.59	0.49	1.32	0.44	1.46	0.45	1.44	0.47
26/06/2017	1.61	0.96	1.56	0.99	1.63	0.97	1.58	0.98	1.57	0.98	1.57	0.98	1.64	0.97	1.66	0.80	1.52	1.00	1.49	1.01
11/12/2017	2.59	1.28	2.77	1.10	2.70	1.05	2.90	1.03	2.76	1.08	2.66	1.11	2.71	1.16	2.55	0.77	2.92	1.02	2.82	1.09
Average	2.34	0.90	2.30	0.85	2.40	0.88	2.37	0.86	2.37	0.86	2.29	0.85	2.34	0.89	2.20	0.74	2.33	0.83	2.31	0.85
Total	2.34	0.90	2.30	0.85	2.40	0.88	2.37	0.86	2.37	0.86	2.29	0.85	2.34	0.89	2.20	0.74	2.33	0.83	2.31	0.85

Table 4
RMSE of the WRF simulation and of the WRF + HDWind simulation using different microphysics parameterizations.

Microphysics	Ferrier		Godddard		Kessler		Lin		Morrison		Thomson		WSM3		WSM5		WSM6		WDM5	
Date	WRF	WRF + HDWind	WRF	WRF + HDWind	WRF	WRF + HDWind	WRF	WRF + HDWind	WRF	WRF + HDWind	WRF	WRF + HDWind	WRF	WRF + HDWind	WRF	WRF + HDWind	WRF	WRF + HDWind	WRF	WRF + HDWind
15/03/2017	1.90	1.16	1.99	1.15	1.88	1.19	2.10	1.18	2.31	1.18	2.02	1.13	1.88	1.20	2.07	0.89	2.06	1.09	2.08	1.08
11/05/2017	3.83	1.14	3.71	1.16	4.03	1.21	3.74	1.15	3.78	1.15	3.76	1.15	3.81	1.17	3.49	1.16	3.73	1.18	3.77	1.20
12/05/2017	3.56	1.04	3.41	0.96	3.65	1.09	3.48	1.04	3.47	1.02	3.31	0.93	3.51	1.05	3.17	1.13	3.26	0.95	3.31	0.99
13/05/2017	2.02	0.62	1.73	0.58	2.05	0.61	1.80	0.59	1.73	0.57	1.71	0.60	1.96	0.61	1.60	0.54	1.72	0.55	1.71	0.58
26/06/2017	1.82	1.12	1.78	1.14	1.85	1.13	1.81	1.14	1.80	1.14	1.79	1.14	1.85	1.12	1.88	0.94	1.73	1.16	1.72	1.18
11/12/2017	2.89	1.82	3.11	1.54	3.08	1.46	3.21	1.48	3.07	1.51	2.96	1.53	3.01	1.62	2.86	1.14	3.24	1.47	3.14	1.53
Average	2.67	1.15	2.62	1.09	2.75	1.11	2.69	1.10	2.69	1.10	2.59	1.08	2.67	1.13	2.51	0.97	2.62	1.07	2.62	1.09
Total	2.79	1.20	2.74	1.13	2.89	1.14	2.81	1.13	2.81	1.13	2.71	1.11	2.79	1.17	2.61	0.99	2.75	1.10	2.75	1.13

Histogram of WRF absolute errors

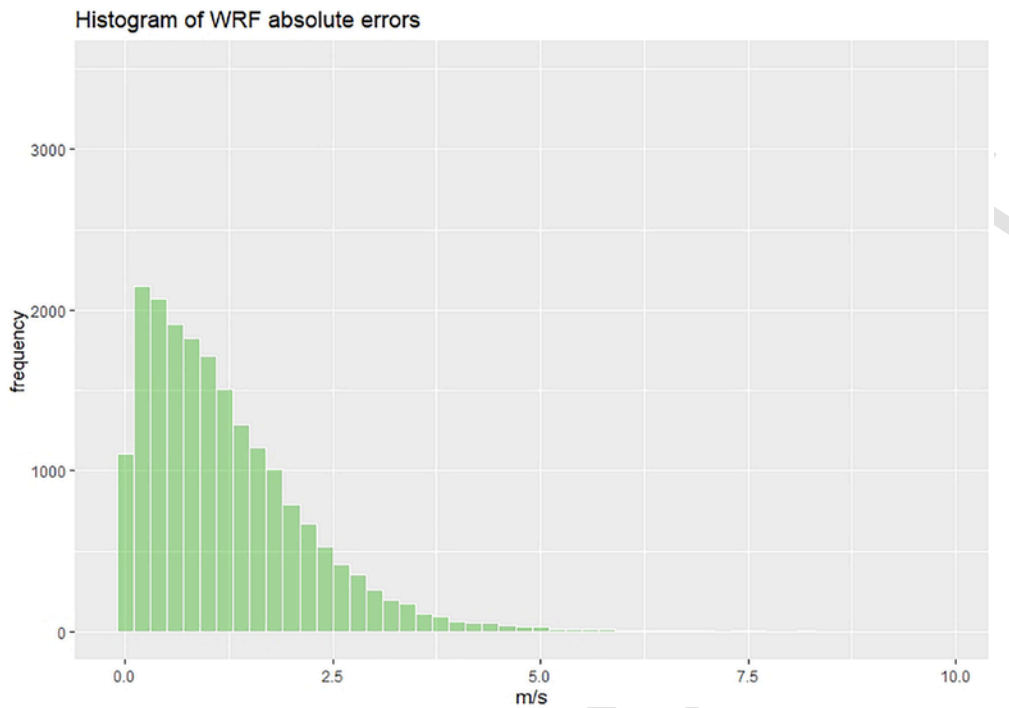**Fig. 8.** Histogram of WRF absolute errors.

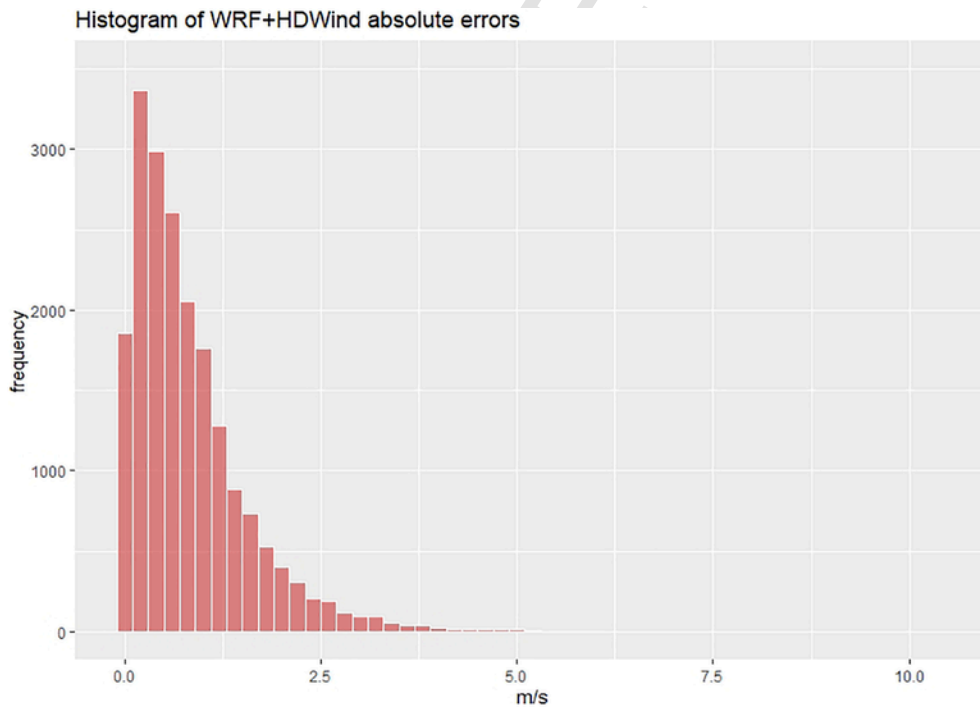### Histogram of WRF+HDWind absolute errors

Fig. 9. Histogram of WRF + HDWind absolute errors.

ment of meteorological wind at the domain boundary, it is enough to provide measurements of wind (intensity and direction) in a reduced set of points in the domain, for example the measurements provided by weather stations.

In Cascón et al. (2016) techniques of reduced basis have been incorporated enabling a much more efficient resolution of the optimal control problem. The reduced basis methodology is especially appropriate in problems in which real-time results are required. The HDWind model was developed under $C++$ using *Neptuno$++$*

, a finite element toolbox developed by some of the authors. In addition, HDWind has been integrated into the ArcGIS Geographic Information System (Prieto et al., 2017) to automate and simplify the geospatial input data and the display of the solutions, and to improve user accessibility.

The details of the model equations exceed the scope of this article, interested readers can find detailed explanations in the aforementioned papers. Its implementation code has been introduced
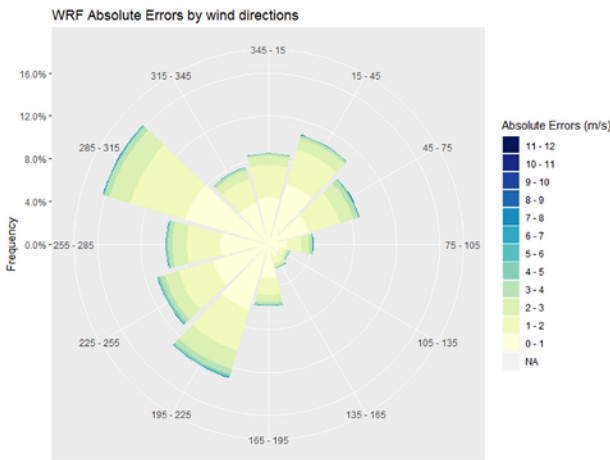
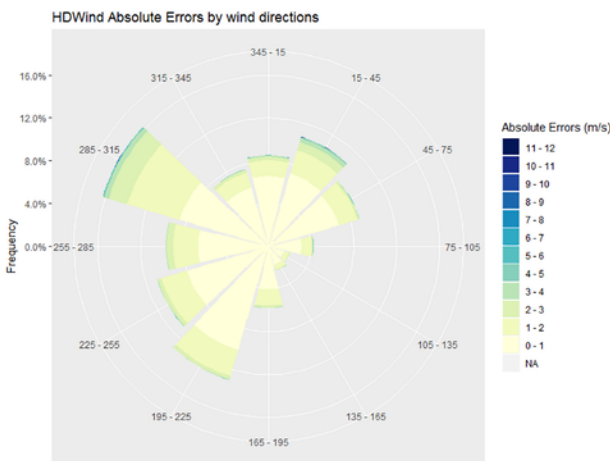**Fig. 10.** Wind rose of WRF absolute errors.

Fig. 11. Wind rose of WRF + HDWind absolute errors.

in the Spanish Intellectual Property Registry on October 18, 2018 under the registration code 00/2019/692.

Fig. 1 summarizes the HDWind inputs (orography, surface roughness, surface temperature distribution and punctual wind measurements), outputs (the wind field at different heights) and parameter (the inverse of the friction coefficient ξ).

2.1.3. WRF-HDWind coupling

As discussed in Section 1, the mesoscale models cannot properly resolve the wind speed induced by the local characteristics such as orography or surface temperature gradients, and the microscale models do not contemplate the atmospheric state beyond their local domain, allowing to simulate not more than a short time period. Being the weather the result of the relationship of a high number of atmospheric factors, the mesoscale models (here the WRF model) are able to predict the hourly wind regime at resolutions of several kilometers, which is adapted to the local characteristics through the use of microscale models (in this case HDWind).

Under this scheme, the predictive information provided by the WRF model is considered, with a medium resolution. On the other hand, the precise conditions of the local domain to be studied, topography and land uses, are incorporated, with a high-resolution, through the simulation with HDWind.

As a result, HDWind provides a high-resolution wind field (see Fig. 2) for successive time instants applicable to a wide range of possibilities: from the transport and diffusion of air pollutants (Ferragut et al., 2013), the prediction of the spread of a wild-

land fire (Asensio et al., 2005), or even the development of time series on the forecast of wind speed and direction to predict the production in a wind farm.

The coupling has been carried out so that the output provided by the WRF model is used as input for the HDWind model. For this, the first step to be performed is to select the local domain for which the high-resolution wind field is going to be calculated.

Next, the WRF model is executed by selecting a broader domain that contains the local domain to be simulated using the HDWind model, preferably in its central zone. WRF allows to simulate or predict the weather conditions that will be used in the simulation with HDWind. In this way, it is possible to perform microscale simulations that cover a broad time period.

Once the simulation or prediction has been carried out, the NetCDF[2] files generated by WRF will be processed to obtain the desired weather conditions, in this case wind direction and intensity, in a reduced set of points contained within the local domain.

With the weather conditions provided by WRF, the HDWind model is executed providing both a 3D wind field and the local wind value at certain points for comparative analysis. Fig. 2 shows the wind field at a certain time instant simulated using the HDWind model. The color of the surface represents the changes in the terrain orography. The complete simulation scenario is described in Section 2.2.

When a time series needs to be simulated to predict behavior over time the proposed procedure needs to repeatedly solve the optimal control problem involved within the HDWind model. When the number of time steps to be simulated is very high, the resolution of this problem can take a considerable amount of time.

In order to solve the problem efficiently, we propose a simply modification of (Cascón et al., 2016). Note first, that the HDWind model requires to solve a linear PDE (see Ferragut et al. (2011)) where the right-hand side depends (linearly) on the wind measurements and the temperature of ground surface. Then, we solve the associated PDE $2 \times n + 1$ times (being n the number of WRF-measures involved in the downscaling) for reference values of wind and for the surface temperature given. For a particular time, the HDWind field can be obtained as linear combination of the solutions previously computed. When the temperature of the ground surface is updated, we only need to solve the corresponding PDE to continue. This procedure is called the superposition method and, in our case, can be applied since orography and wind measurements location are fixed. From the numerical point of view, we use Finite Element Method (FEM) to approximate the HDWind-PDE. The proposed scheme only requires to calculate and factorize once the associate matrix.

2.2. Scenario

The improvement obtained by the downscaling procedure is tested in an urban-interface area from Badajoz, a Spanish city located near the Portugal border. The simulated period runs from January 2, 2017 at 00:00 h local time until February 28, 2018 at 23:30 h local time. The HDWind simulation area includes heterogeneous surfaces with very different roughness: areas with very low roughness, as the river Guadiana, and areas with high roughness, as the urbanized areas from the city of Badajoz, going through areas with intermediate values such as crops and forests. This disparity of roughness (see Fig. 4) makes this scenario a great opportunity for the testing of the proposed procedure, allowing the adjustment
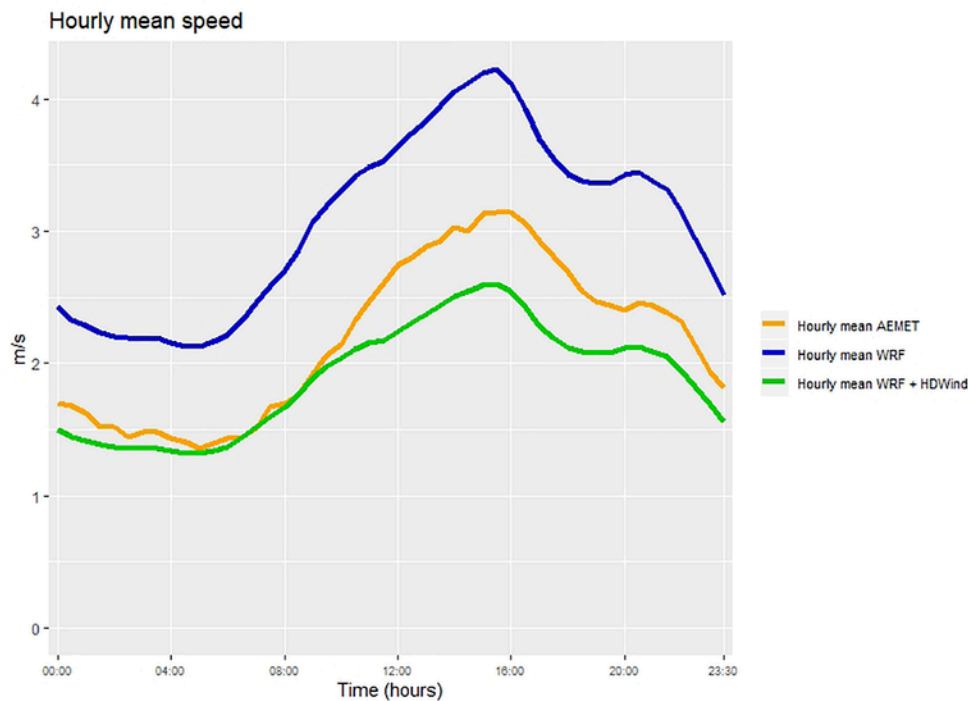

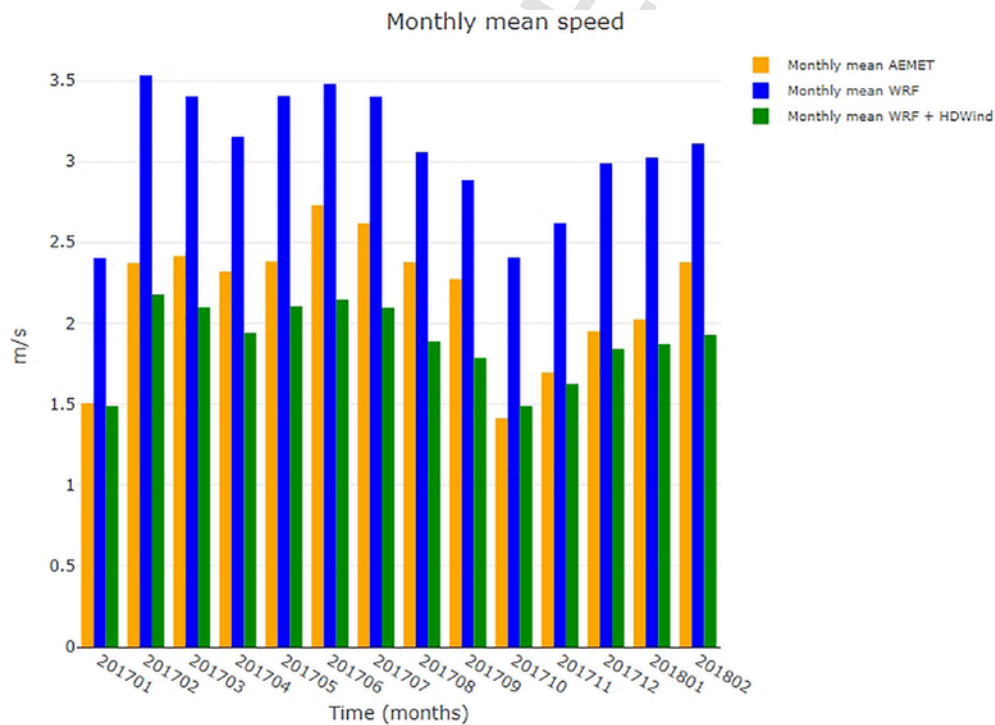
Fig. 12. Hourly mean wind speed.

Fig. 13. Monthly mean wind speed.

of the wind speed forecasts provided by WRF to the local particularities.

2.2.1. WRF set-up

The simulation was performed using the ARW-WRF model to generate wind data forecasts with one day ahead of prediction horizon and with a temporal resolution of 15 min. We have used the WRF version 3.8.1 modified by (Hahmann et al., 2019).

The domain simulated using the ARW-WRF model for the Badajoz region is composed of two one-way nested domains, with increasing resolution, centered at 38.8875° *N*; 7.0117° *W* in the WGS84 coordinates. This point is close to the location of the weathervane tower of the *Spanish State Meteorological Agency* (AEMET). Fig. 5 shows the points where the WRF center and the AEMET weathervane tower are located. These two nested domains are formed with 100x100 points and horizontal resolution of 9 *km*,

Table 5
Statistic errors.

Month-Year	Mean$_{WRF}$	Mean$_{WRF+HDWind}$	Mean$_{AEMET}$	BIAS$_{WRF}$	BIAS$_{WRF+HDWind}$	MAE$_{WRF}$	MAE$_{WRF+HDWind}$	RMSE$_{WRF}$	RMSE$_{WRF+HDWind}$
January 2017	2.40	1.49	1.50	0.90	−0.02	1.15	0.74	1.52	1.00
February 2017	3.53	2.18	2.37	1.16	−0.20	1.36	0.79	1.72	1.05
March 2017	3.40	2.10	2.42	0.99	−0.32	1.28	0.83	1.71	1.15
April 2017	3.15	1.94	2.32	0.83	−0.38	1.14	0.79	1.43	1.03
May 2017	3.40	2.11	2.38	1.02	−0.28	1.31	0.74	1.71	0.97
June 2017	3.48	2.15	2.73	0.75	−0.58	1.30	1.00	1.72	1.33
July 2017	3.40	2.10	2.62	0.78	−0.52	1.16	0.90	1.48	1.20
August 2017	3.06	1.89	2.38	0.68	−0.49	1.15	0.89	1.53	1.20
September 2017	2.88	1.79	2.27	0.61	−0.49	1.02	0.83	1.30	1.07
October 2017	2.41	1.49	1.41	0.99	0.07	1.20	0.64	1.50	0.84
November 2017	2.62	1.62	1.70	0.92	−0.07	1.27	0.85	1.64	1.19
December 2017	2.99	1.84	1.95	1.04	−0.11	1.26	0.72	1.60	0.95
January 2018	3.02	1.87	2.02	1.00	−0.15	1.25	0.81	1.61	1.08
February 2018	3.11	1.93	2.38	0.73	−0.45	1.18	0.98	1.55	1.36
Total Period	3.07	1.89	2.18	0.89	−0.29	1.22	0.82	1.58	1.11
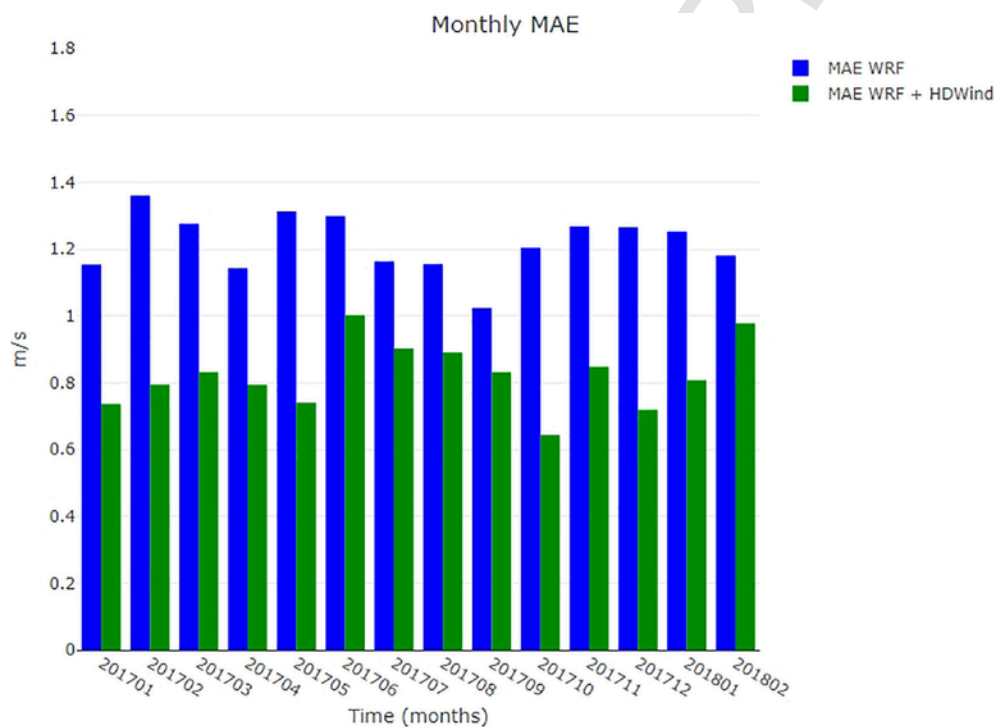
Fig. 14. Monthly MAE (Mean Absolute Error).

the largest one, and 88x88 points and horizontal resolution of 3 *km*, the smallest one, and are represented in Fig. 3. Each of these two domains has 35 vertical levels from the surface to the top of the atmosphere, located at the constant pressure surface of 25 *mbar* ($\approx$ 20 *km*). The running time of the WRF model in the HPC (*High Performance Computer*) cluster composed by 24 CPUs Intel(R) Xeon(R) Gold 6126 CPU @ 2.60GHz with 128Gb of RAM was approximately 3 h (GFS download + pre-process + execution) per simulated day. In total, the WRF simulation required 1269 h of computing.

Finally, the election of all the physics parameterizations, summarized in Table 1, was based on results from the New European Wind Atlas (NEWA) project[3]. These results were validated in hundreds of points across Europe and the physics setup with the lowest wind speed errors was chosen (Hahmann et al., 2019). The

WRF setup used in this work is virtually identical to the one obtained in the NEWA project, apart from the lower number of vertical levels and the use of GFS input data, instead of reanalysis data. We tested two WRF setups using different number of vertical levels, that is, 61 as recommended in (Hahmann et al., 2019) and 35 vertical levels. Since the results don't show any significant improvement for the case of study when we use a higher number of vertical levels, we chose the WRF setup which uses 35 vertical levels because it also allowed to reduce the computational cost. We consider that the reason why the use of a greater number of vertical levels does not provide an improvement may be due to the fact that the output of the WRF model is located on a crop field while the observation is carried out in an urbanized area with greater effective roughness (See Fig. 5). In this scenario, the limitation of mesoscale models when applied in heterogeneous terrain is appreciated, to which we propose a solution in this paper by combining mesoscale and microscale models.

Real-time Global Forecasting System (GFS) data from the 1200 UTC cycle and a horizontal resolution of 0.25° are used to feed
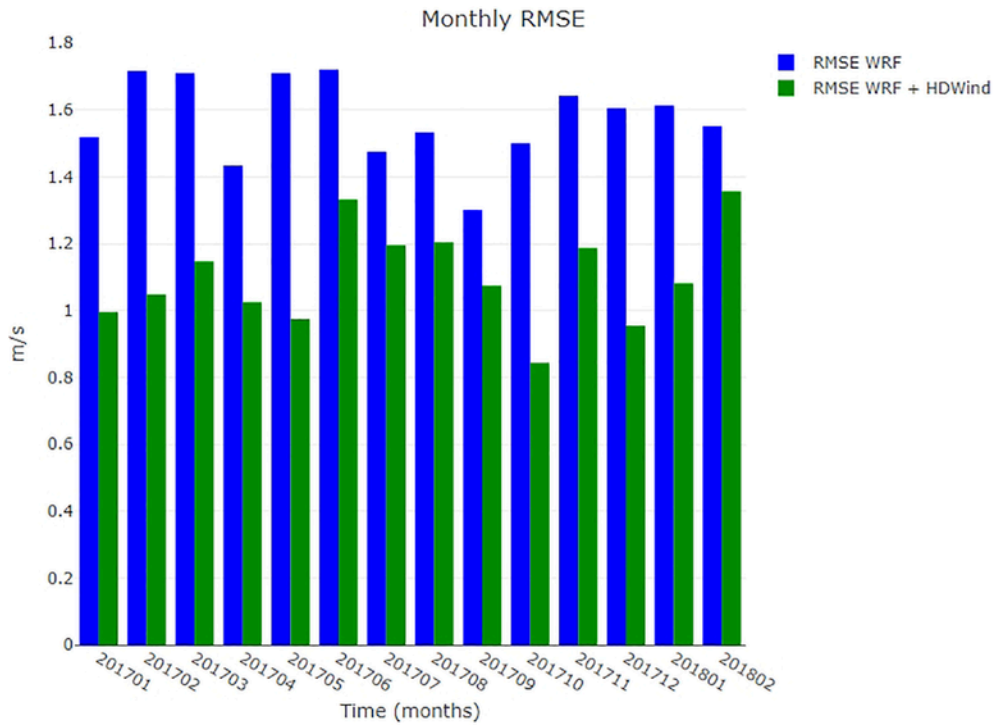
---

[3] http://www.neweuropeanwindatlas.eu

Fig. 15. Monthly RMSE (Root Mean Square Error).

Table 6
Monthly correlation coefficients.

Month-Year	Correlation coefficient$_{WRF}$	Correlation coefficient$_{WRF + HDWind}$
January 2017	0.67	0.67
March 2017	0.77	0.77
April 2017	0.77	0.77
May 2017	0.76	0.76
June 2017	0.76	0.76
July 2017	0.67	0.67
August 2017	0.67	0.67
September 2017	0.67	0.67
October 2017	0.75	0.75
November 2017	0.57	0.57
December 2017	0.55	0.55
January 2018	0.81	0.81
February 2018	0.74	0.74
Total Period	**0.72**	**0.72**

the daily real time WRF simulations. This data, with a horizon of 48 hours and 3 hours frequency, are used in each simulation to generate the day ahead meteorological forecasts.

Updated land cover from Corine (2012) with a horizontal resolution of 100 *m* together with high-resolution topography data from the Shuttle Radar Topography Mission (SRTM) with 90 *m* horizontal resolution are used instead of the default land cover and topography provided by the WRF model. The use of high-resolution static data has proven to improve the WRF general accuracy in multiple locations and different types of terrain (Cheng et al., 2013; Correia et al., 2013; Ki Kim et al., 2019; Kirthiga and Patel, 2018).

2.2.2. HDWind set-up

The simulation domain used for the HDWind model also has the center located near the weathervane tower of AEMET, with latitude 38.8873° *N* and longitude 7.0093° *W* in the WGS84 coordinates. This point is halfway between the location of the AEMET weather station and the point at which WRF data are extracted. The HDWind domain mesh has a resolution of 10 meters and 795*x*752 elements, which is a domain of almost 8*x*8 *km* (see Fig. 4).

The HDWind model has been provided with terrain altimetry data from the *Digital Elevation Model* MDT05 (IGN, 2013) published by the *Spanish National Geographic Institute* (IGN) and land use data from the *Spanish Forestry Map* 1: 50,000 (MFE50) (Magrama, 2007) developed by the *Ministry of Agriculture, Food and Environment* of the Spanish Government. The surface temperature has been considered constant given the impossibility of obtaining soil temperature data with sufficient temporal resolution (30 min).

The HDWind simulation was carried out in two stages. In a first step, the January 2017 data were used to adjust the inverse of the friction coefficient ξ as function of the surface roughness length z_0:

$$\xi = f(z_0) := \frac{1}{a_0 + a_1 z_0 + a_2 z_0^2} \tag{1}$$

The coefficients $\{a_0, a_1, a_2\}$ were computed to minimize the root mean square error (RMSE) between AEMET-measured and HD-Wind-computed velocities at the first month (January 20,017). The roughness length z_0 comes from the classification of land uses and its correspondence with the classification of Davenport et al. (2000) (see Fig. 4). To solve this optimization problem a method based on the golden-section search was used. The computational cost for the adjustment was about 20 hours on a workstation equipped with two Intel(R) Xeon(R) E5–2670 v2 processors (10 cores, each working at a frequency of 2.50 GHz) and 64 GB RAM.
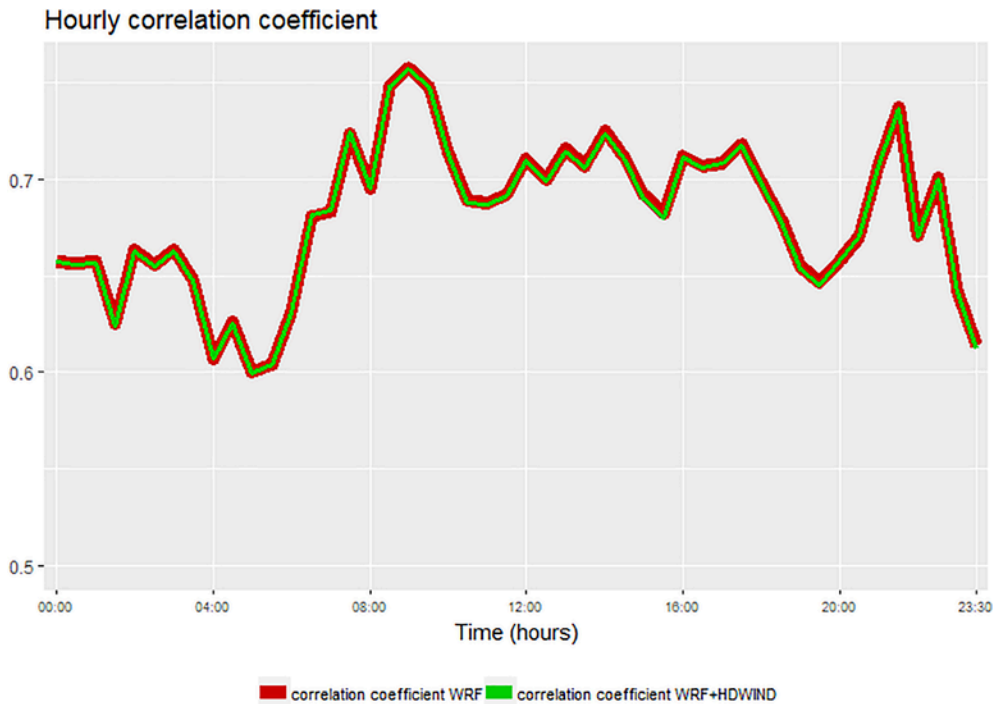
Hourly correlation coefficient

correlation coefficient WRF · correlation coefficient WRF+HDWIND

Fig. 16. Hourly correlation coefficients.

In a second step, the ARW-WRF data were used by the HDWind model to perform the downscaling throughout the entire study period (423 days). The strategy to compute the HDWind field, that was mentioned at Section 2.1.3, allows to obtain the results at the simulated period covered in about 20 minutes on the same workstation. Note that although the parallelization of this computation is possible, this calculation has been performed sequentially.

The data generated by the WRF model used as input to the HDWind model were extracted at the central point of the simulation domain (38.8875° N,7.0117° W) and at a surface height of 80 m, that is, the nearest point on the WRF mesh to the weather station with whose observations the data is compared. This weather station is located at coordinates Latitude 38, 8860° N Longitude 7.0092° W and at an altitude of 175 m above sea level (See Fig. 5).

3. Results

For the evaluation of the procedure involving the coupling of the WRF-HDWind models, both the wind speed forecasts obtained by WRF and the high-resolution wind field provided by the joint operation of the WRF + HDWind models are compared with the measurements read by a weathervane tower of AEMET over the period of time which goes from January 2, 2017 at 00:00 h local time until February 28, 2018 at 23:30 h with a temporal resolution of 30 min. For this comparison, both the results of the WRF simulation and the joint operation of the WRF + HDwind models were extracted at the AEMET station location and at a surface height of 10 m. To make the comparison, the three typical error statistics have been used, that is the BIAS (eq. 2), the Mean Absolute Error (MAE) (eq. 3), and the Root Mean Square Error (RMSE) (eq. 4). Besides, different graphics that highlight the improvement obtained over the initial meteorological forecasts have been made.

$$BIAS = \frac{\sum_{i=1}^{N} (V_i - P_i)}{N} \quad (2)$$

$$MAE = \frac{\sum_{i=1}^{N} |V_i - P_i|}{N} \quad (3)$$

$$RMSE = \frac{\sqrt{\sum_{i=1,n} (V_i - P_i)^2}}{N} \quad (4)$$

Where V_i refers to the $i-th$ observation of wind speed and P_i corresponds to the predicted value.

So, the first analysis consists of a heat map that allows the visualization of all data deviation in a unique plot. The X axis refers to each one of the days predicted in our study period meanwhile the Y axis contains each 30-min data predicted (48 data per day). The color intensity corresponds to the level of absolute error (AE) presented by the prediction. Fig. 6 contains the deviations presented by the WRF simulation meanwhile the Fig. 7 presents the deviations from the WRF + HDWind models. It is clear that, in general, the intensity of the WRF + HDWind errors is much less than those presented by the WRF, showing in case of WRF + HDWind major areas with low error levels reflected in the greater clarity of the plot. Also, Figs. 6 and 7 show that errors are concentrated in certain days pointing out some episodes less predictable. In order to understand these episodes, the correlation between errors and the daily summary of the AEMET-measurements has been studied. The results show that the error observed in these less predictable episodes is mainly related to wind gust and to a lesser extent to precipitations.

It is important to note that the time slot of the day in which the models WRF + HDWind have a lower level of error corresponds to night-time hours. This behavior is due to the fact that a uniform surface temperature value has been used for the whole study period as explained in Section 2.2.2, a situation that does not correspond to reality and that will be addressed in future works.

Since the WRF setup used to obtain the predictive information is a recommended generic configuration (Hahmann et al., 2019), we have selected 6 days with the highest accumulated error and

we have applied the same simulation process: using the WRF mesoscale model and subsequent downscaling with the HDWind microscale model and different microphysics parameterizations of the WRF model. The objective is to assess the impact of having used a generic WRF setup (see section 2.2.1) and verify if any other configuration would have been more appropriate for our case of study. The tested microphysics parameterizations are: Ferrier, Godddard, Kessler, Lin, Morrison, Thomson, WRF Single-Moment 3-class (WSM3), WRF Single-Moment 5-class (WSM5), WRF Single-Moment 6-class (WSM6), WRF Double-Moment 5-class (WDM5) and WRF Double-Moment 6-class (WDM6).

The results show that although there are days that are better represented by other setups than the initial one, we have verified that for these 6 days, in general, the original setup is the one that best fits. The errors obtained of all WRF setups tested are summarized in Tables 2, 3 and 4, which contain the AE, the MAE and the RMSE errors respectively. Furthermore, these tables also collect the errors obtained in the downscaling using the HDWind microscale model (when it is fed with predictive information provided by the different WRF setups). It is important to note that the combination of the WRF and HDWind models improves the result in all the cases considered, and specially that the worst result of the joint operation of both models improves significantly the best result of the isolated operation of the WRF mesoscale model. Thus, it might be concluded that the joint operation of the WRF and HDWind models allows obtaining an accurate estimate of the wind intensity even though an optimal configuration of the WRF model has not been chosen for the study scenario.

In the same line, the histogram is another useful graphic tool to compare the absolute errors of the predictions for each time step. So, Fig. 8 contains the histogram related to the WRF deviations meanwhile the WRF + HDWind ones are compiled in the Fig. 9. It can be seen how the histogram from WRF + HDWind errors presents a major frequency of data with low values meanwhile the WRF histogram presents a less pointed distribution with major frequency of higher absolute errors.

To complete the performance comparison, we have also carried out an error analysis using wind direction as a ranking factor. This type of analysis is very useful to identify possible systematic errors caused in specific cases that depend of wind direction and to highlight if different behavior can be assumed depending of wind regime. As a result, Figs. 10 and 11 contain the respective wind rose graphics for absolute errors of both models, WRF and WRF + HDWind. It is observed that, for both of them, the absolute error distributions are quite similar for different sections of wind direction for our case of study. Besides, it is important to remark that the absolute error decrease obtained by the WRF + HDWind coupling is also observed, but this decrease is more significative when wind comes from south and surrounds for our case of study. The wind from these directions is characterized by crossing very heterogeneous areas, such as urban areas, crop fields or the Guadiana river.

The tests carried out on the joint operation of the WRF + HDWind models show that the proposed method solves one of the problems that the WRF model presents when it is applied by itself to the area selected for the study, which is the overestimation of wind speed. Some users have experienced a similar behavior when it is applied to areas of complex terrain (Cheng and Steenburgh, 2005; El-Samra et al., 2018; Gómez-Navarro et al., 2015; Hahmann et al., 2019; Jiménez et al., 2012; Mass and Ovens, 2011; Solbakken and Birkelund, 2018). So, when mean wind speed are compared this fact is clearly observed. The case of the daily profile, that is the mean wind speed observed by each 30 min over all data of the period, is collected in Fig. 12 where the blue line corre-

sponds to the WRF data, the green one to the WRF + HDWind data and the orange line is the real data from the AEMET meteorological station. It is clear how the wind speed is in general overestimated by the WRF model meanwhile the mean offered by WRF + HDWind is more similar to the real data. One possible explanation for the overestimation of the wind intensity values obtained during the simulation of this scenario is that this may be due to the heterogeneity of the terrain that limits the accuracy obtained from the WRF mesoscale model. As mentioned above, the point of the WRF mesh closest to the observation station, where the data has been extracted, and the observation station are located on different land uses. In fact, the output of the WRF model is located on a crop field while the observation was carried out in an urbanized area. The same situation is observed when monthly data are analyzed as can be seen in Fig. 13. Our proposal solves this limitation of the mesoscale models when applied to heterogeneous terrain through the combination of mesoscale and microscale models. Report once again the difference in the level of error values obtained in WRF + HDWind between daytime and night-time hours.

The general improvement obtained by the WRF + HDWind is clearly showed by the statistic errors calculated in our time period. All data are compiled in the Table 5, both monthly information and the total one. Besides it contains the respective mean speed measured and predicted by each model. Therefore, the three deviation measurements are reduced: in case of BIAS the data obtained by WRF + HDWind presents −0.29 *m/s* in front of the 0.89 *m/s* of the WRF data. The MAE of the WRF + HDWind achieves a value of 0.82 *m/s* in front of 1.22 *m/s* obtained by WRF and, to finish, the RMSE presented by WRF + HDWind has a value of 1.11 *m/s* meanwhile WRF offers 1.58 *m/s*.

Moreover, if we analyze the deviation observed by months, we can see how all of monthly results are improved after using the HDWind model, achieving less than 1 *m/s* of MAE in all months and under 1.4 *m/s* in terms of RMSE. The improvement of the WRF + HDWind achieves up to 40% of error decreasing in terms of MAE in months as February 2017 or October 2017. The same situation can be seen in terms of RMSE. So, Fig. 14 contains the monthly MAE obtained by WRF (blue bars) and by WRF + HDWind (green bars) and Fig. 15 the respective monthly RMSE with the same colors.

To complete the comparison of WRF and WRF + HDWind simulations we have evaluated the correlation coefficients between each model and the respective real data. So, as it is shown in Table 6, the correlation coefficient achieves a value of 0.72 in both cases. The monthly discrimination shows on the one hand, that both models present the same level of correlation with practically equal values in all months and, on the other hand, that the correlation achieves values greater than 0.75 in a half of the months being around 0.7 in practically the rest. The same situation is observed when we make the analysis by daily hours. The results of correlation coefficients observed when only data from each daily instant are used, can be seen in Fig. 16. It shows how both models present practically the same correlation with measured data along the day.

Note that the results show that the roughness coefficients adjustment mentioned in Section 2.2.2 is robust and independent of wind data. Although only the January 2017 data were used in this adjustment the correlation between AEMET-measurement and WRF + HDWind-simulated is high satisfactory all along period covered.

4. Discussion and conclusions

During the development of this work, two Numerical Weather Prediction models, the WRF mesoscale model and the HDWind mi-

croscale model, have been coupled for the accurate estimation of a wind field that meets the local characteristics of the terrain.

For their coupling, both models have been studied and analyzed. Next, a dynamic downscaling has been carried out in which HDWind uses geolocalized data of wind speed and direction as input data, obtained by the execution of the WRF model.

The proposed procedure has been applied to an area located in the urban-interface of the city of Badajoz (Spain). Note that this method can be applied along the globe by simply feeding the models with the appropriate spatial information to represent the local characteristics of the terrain. The results have been compared with the measurements recorded by a physical anemometer of AEMET. The results obtained show that the joint operation of the WRF + HDWind models allows to reduce the margin of error up to 40% with respect to the execution of the WRF model by itself.

Different microphysics parameterizations of the WRF model has been tested in order to assess the impact of having used a generic WRF setup. Results show that the combination of the WRF and HDWind models improves the result in all the cases considered, and specially that the worst result of the joint operation of both models improves significantly the best result of the isolated operation of the WRF mesoscale model. Thus, it might be concluded that the joint operation of the WRF and HDWind models allows obtaining an accurate estimate of the wind intensity even though an optimal configuration of the WRF model has not been chosen for the study scenario.

A problem detected in the wind intensity values obtained by the WRF model for the study domain is the overestimation of the wind speed. The tests carried out on the joint operation of the WRF + HDWind model shows that the proposed method is able to solve this problem. A possible explanation for the overestimation may be due to the fact that the point of the WRF mesh closest to the observation station is located on a crop field while the observation is carried out in an urbanized area with greater effective roughness. Under this scenario, the limitations of mesoscale models when applied in heterogeneous terrain are appreciated.

In addition, the statistical analysis of the data shows that the joint operation of the WRF + HDWind models provides a more accurate wind field in the study area, especially during the night-time hours. Although the HDWind model allows to consider the temperature gradients on the surface, that is to incorporate the local heating and cooling of the surface due for example to solar radiation, the state of the art of satellite image analysis and other remote sensing techniques does not allow us to generate this information with sufficient temporal resolution. We consider the use of constant surface temperature the cause of the greatest deviation during daily hours.

It is important to note that the computational cost added by the use of the HDWind model is significantly lower than the cost of executing the WRF mesoscale model, so that there is not a significant increase in the time required to carry out the simulation of a wind field.

The improvement obtained in the prediction of the meteorological wind intensity can contribute significantly to go a step further in other areas where the meteorological wind is an important factor, such as the spread of forest fires or the dispersion of pollutants in the atmosphere.

CRediT authorship contribution statement

D. Prieto-Herráez: Conceptualization, Methodology, Validation, Formal analysis, Investigation, Data curation, Writing - original draft, Writing - review & editing, Visualization, Project administration. **L. Frías-Paredes:** Conceptualization, Methodology, Validation, Formal analysis, Investigation, Data curation, Writing - original draft, Writing - review & editing, Visualization, Project administration, Funding acquisition.

J.M. Cascón: Conceptualization, Methodology, Software, Investigation, Writing - review & editing, Visualization, Project administration. **S. Lagüela-López:** Resources, Investigation, Writing - review & editing, Funding acquisition. **M. Gastón-Romeo:** Resources, Investigation, Data curation, Writing - review & editing, Visualization. **M.I. Asensio-Sevilla:** Writing - review & editing, Funding acquisition. **I. Martín-Nieto:** Resources, Writing - review & editing. **P.M. Fernandes-Correia:** Resources, Investigation, Data curation, Writing - review & editing, Visualization. **P. Laiz-Alonso:** Resources, Writing - review & editing. **O.F. Carrasco-Díaz:** Software, Writing - review & editing, Funding acquisition. **C. Sáez-Blázquez:** Resources, Writing - review & editing. **E. Hernández:** Writing - review & editing, Supervision. **L. Ferragut-Canals:** Writing - review & editing, Supervision. **D. González-Aguilera:** Writing - review & editing, Supervision, Funding acquisition.

Declaration of Competing Interest

The authors declare that they have no known competing financial interests or personal relationships that could have appeared to influence the work reported in this paper.

Acknowledgments

References

Arakawa, A., Konor, C.S., 1996. Vertical differencing of the primitive equations based on the Charney–Phillips grid in hybrid &sigma–p vertical coordinates. Mon. Weather Rev. 124, 511–528. https://doi.org/10.1175/1520-0493(1996)124<0511:VDOTPE>2.0.CO;2.

Asensio, M.I., Ferragut, L., Simon, J., 2005. A convection model for fire spread simulation. Appl. Math. Lett. 18, 673–677 http://www.sciencedirect.com/science/article/pii/S0893965904003787 https://doi.org/10.1016/j.aml.2004.04.011, (Special issue on the occasion of MEGA 2003).

Cascón, J.M., Engdahl, A., Ferragut, L., Hernández, E., 2016. A reduced basis for a local high definition wind model. Comput. Methods Appl. Mech. Eng. 311, 438–456 http://www.sciencedirect.com/science/article/pii/S0045782516302912 https://doi.org/10.1016/j.cma.2016.08.028.

Cheng, W.Y.Y., Steenburgh, W.J., 2005. Evaluation of surface sensible weather forecasts by the WRF and the ETA models over the Western United States. Weather Forecast. 20, 812–821. https://doi.org/10.1175/WAF885.1.

Cheng, F.Y., Hsu, Y.C., Lin, P.L., Lin, T.H., 2013. Investigation of the effects of different land use and land cover patterns on mesoscale meteorological simulations in the Taiwan area. J. Appl. Meteorol. Climatol. 52, 570–587. https://doi.org/10.1175/JAMC-D-12-0109.1.

Correia, P., Lozano, S., Chavez, R., Loureiro, Y., Cantero, E., Benito, P., Sanz, J., 2013. Wind characterization at the Alaiz-Las Balsas experimental wind farm using high-resolution simulations with mesoscale models. Development of a "low cost" methodology that address promoters needs. In: EWEA-13 Proceedings. European Wind Energy Conference, EWEA volume, Vienna, p. 3, (p. 1818).

Davenport, A.G., Grimmond, C.S.B., Oke, T.R., Wieringa, J., 2000. Estimating the roughness of cities and sheltered country. In: Preprints Twelfth Conference on Applied Climatology. American Meteorological Society, pp. 96–99.

El-Samra, R., Bou-Zeid, E., El-Fadel, M., 2018. What model resolution is required in climatological downscaling over complex terrain?. Atmos. Res. 203, 68–82 http://www.sciencedirect.com/science/article/pii/S0169809516305798 https://doi.org/10.1016/j.atmosres.2017.11.030.

Fernández-González, S., Martín, M.L., García-Ortega, E., Merino, A., Lorenzana, J., Sánchez, J.L., Valero, F., Sanz-Rodrigo, J., 2018. Sensitivity analysis of the WRF model: Wind-resource assessment for complex terrain. J. Appl. Meteorol. Climatol. 57, 733–753. https://doi.org/10.1175/JAMC-D-17-0121.1.

Ferragut, L., Asensio, M.I., Simon, J., 2011. High definition local adjustment model of 3D wind fields performing only 2D computations. Int. J. Numer. Methods Biomed. Eng. 27, 510–523. https://doi.org/10.1002/cnm.1314.

Ferragut, L., Asensio, M.I., Cascón, J.M., Prieto, D., Ramírez, J., 2013. An efficient algorithm for solving a multi-layer convection–diffusion problem applied to air pollution problems. Adv. Eng. Softw. 65, 191–199 http://www.sciencedirect.com/science/article/pii/S0965997813001087 https://doi.org/10.1016/j.advengsoft.2013.06.010.

Frías-Paredes, L., Mallor, F., Gastón-Romeo, M., León, T., 2016. Introducing the temporal distortion index to perform a bidimensional analysis of renewable energy forecast. Energy 94, 180–194 http://www.sciencedirect.com/science/article/pii/S0360544215014619 https://doi.org/10.1016/j.energy.2015.10.093.

Frías-Paredes, L., Mallor, F., Gastón-Romeo, M., León, T., 2017. Assessing energy forecasting inaccuracy by simultaneously considering temporal and absolute errors. Energy Convers. Manag. 142, 533–546 http://www.sciencedirect.com/science/article/pii/S0196890417302674 https://doi.org/10.1016/j.enconman.2017.03.056.

Frías-Paredes, L., Mallor, F., Gastón-Romeo, M., León, T., 2018. Dynamic mean absolute error as new measure for assessing forecasting errors. Energy Convers. Manag. 162, 176–188 http://www.sciencedirect.com/science/article/pii/S0196890418301341 https://doi.org/10.1016/j.enconman.2018.02.030.

Gómez-Navarro, J. J., Raible, C. C., & Dierer, S. (2015). Sensitivity of the WRF model to PBL parametrisations and nesting techniques: evaluation of wind storms over complex terrain. Geosci. Model Dev., 8, 3349–3363. URL: https://www.geosci-model-dev.net/8/3349/2015. doi: https://doi.org/10.5194/gmd-8-3349-2015.

Gopalan, H., Gundling, C., Brown, K., Roget, B., Sitaraman, J., Mirocha, J.D., Miller, W.O., 2014. A coupled mesoscale–microscale framework for wind resource estimation and farm aerodynamics. J. Wind Eng. Ind. Aerodyn. 132, 13–26 http://www.sciencedirect.com/science/article/pii/S016761051400107X https://doi.org/10.1016/j.jweia.2014.06.001.

Hahmann, A.N., Witha, B., Sile, T., Dörenkaemper, M., Söderberg, S., Navarro, J., Leroy, G., Folch, A., García-Bustamante, E., Gonzalez-Rouco, F., 2019. WRF Sensitivity Experiments for the Mesoscale NEWA Wind Atlas Production Run. https://doi.org/10.5281/zenodo.2682604.

Hari-Prasad, K., Srinivas, C., Narayana-Rao, T., Naidu, C., Baskaran, R., 2017. Performance of WRF in simulating terrain induced flows and atmospheric boundary layer characteristics over the tropical station gadanki. Atmos. Res. 185, 101–117 http://www.sciencedirect.com/science/article/pii/S0169809516305191 https://doi.org/10.1016/j.atmosres.2016.10.020.

Hong, S.Y., Dudhia, J., Chen, S.H., 2004. A revised approach to ice microphysical processes for the bulk parameterization of clouds and precipitation. Mon. Weather Rev. 132, 103–120. https://doi.org/10.1175/1520-0493(2004)132<0103:ARATIM>2.0.CO;2.

Iacono, M.J., Delamere, J.S., Mlawer, E.J., Shephard, M.W., Clough, S.A., Collins, W.D., 2008. Radiative forcing by long-lived greenhouse gases: calculations with the AER radiative transfer models. J. Geophys. Res. 113, https://doi.org/10.1029/2008JD009944, https://agupubs.onlinelibrary.wiley.com/doi/abs/10.1029/2008JD009944.

IGN, 2013. Spanish Digital Elevation Model. Available via a Web Coverage Service from http://www.ign.es/wcs/mdt.

Jiménez, P.A., Dudhia, J., González-Rouco, J.F., Navarro, J., Montávez, J.P., García-Bustamante, E., 2012. A revised scheme for the WRF surface layer formulation. Mon. Weather Rev. 140, 898–918. https://doi.org/10.1175/MWR-D-11-00056.1.

Kain, J.S., 2004. The Kain–Fritsch convective parameterization: an update. J. Appl. Meteorol. 43, 170–181. https://doi.org/10.1175/1520-0450(2004)043<0170:TKCPAU>2.0.CO;2.

Ki Kim, C., Yum, S., Kim, H.-G., Kang, Y.-H., 2019. A WRF modeling study on the effects of land use changes on fog off the west coast of the Korean Peninsula. Pure Appl. Geophys. 1–18. https://doi.org/10.1007/s00024-019-02242-z.

Kirthiga, S., Patel, N., 2018. Impact of updating land surface data on micrometeorological weather simulations from the WRF model. Atmósfera 31, 165–183 https://www.revistascca.unam.mx/atm/index.php/atm/article/view/ATM.2018.31.02.05 10.20937/ATM.2018.31.02.05.

Klemp, J.B., Skamarock, W.C., Dudhia, J., 2007. Conservative split-explicit time integration methods for the compressible nonhydrostatic equations. Mon. Weather Rev. 135, 2897–2913. https://doi.org/10.1175/MWR3440.1.

Laprise, R., 1992. The Euler equations of motion with hydrostatic pressure as an independent variable. Mon. Weather Rev. 120, 197–207. https://doi.org/10.1175/1520-0493(1992)120<0197:TEEOMW>2.0.CO;2.

Liu, Y., Ren, H.L., 2015. A hybrid statistical downscaling model for prediction of winter precipitation in China. Int. J. Climatol. 35, 1309–1321 https://rmets.onlinelibrary.wiley.com/doi/abs/10.1002/joc.4058 https://doi.org/10.1002/joc.4058.

Magrama, 2007. Spanish Forestry Map 1:50,000. Available from https://www.miteco.gob.es/es/biodiversidad/servicios/banco-datos-naturaleza/informacion-disponible/mfe50.aspx.

Manor, A., Berkovic, S., 2015. Bayesian inference aided analog downscaling for near-surface winds in complex terrain. Atmos. Res. 164-165, 27–36 http://www.sciencedirect.com/science/article/pii/S0169809515001167 https://doi.org/10.1016/j.atmosres.2015.04.014.

Mass, C., & Ovens, D. (2011). Fixing WRF's high speed wind bias: a new subgrid scale drag parameterization and the role of detailed verification. Am. Meteorol. Soc., https://ams.confex.com/ams/91Annual/

webprogram/Paper180011.html. 24th Conference on Weather and Forecasting/20th Conference on Numerical Weather Prediction.

Michalakes, J., Chen, S., Dudhia, J., Hart, L., Klemp, J., Middlecoff, J., Skamarock, W., 2001. Development of a next generation regional weather research and forecast model. In: Developments in Teracomputing. Ninth ECMWF Workshop on the Use of High Performance Computing in Meteorology pp. 269–276. https://doi.org/10.1142/9789812799685_0024.

Mughal, M.O., Lynch, M., Yu, F., Sutton, J., 2018. Forecasting and verification of winds in an East African complex terrain using coupled mesoscale and microscale models. J. Wind Eng. Ind. Aerodyn. 176, 13–20 http://www.sciencedirect.com/science/article/pii/S0167610517309935 https://doi.org/10.1016/j.jweia.2018.03.006.

Nakanishi, M., Niino, H., 2009. Development of an improved turbulence closure model for the atmospheric boundary layer. J. Meteorol. Soc. Japan Ser. II 87, 895–912. https://doi.org/10.2151/jmsj.87.895.

Oliver, A., Rodríguez, E., Escobar, J.M., Montero, G., Hortal, M., Calvo, J., Cascón, J.M., Montenegro, R., 2015. Wind forecasting based on the HARMONIE model and adaptive finite elements. Pure Appl. Geophys. 172 (1), 109–120 https://link.springer.com/article/10.1007/s00024-014-0913-9 https://doi.org/10.1007/s00024-014-0913-9.

Ooyama, K.V., 1990. A thermodynamic foundation for modeling the moist atmosphere. J. Atmos. Sci. 47, 2580–2593. https://doi.org/10.1175/1520-0469(1990)047<2580:ATFFMT>2.0.CO;2.

Orlanski, I., 1975. A rational subdivision of scales for atmospheric processes. Bull. Am. Meteorol. Soc. 56, 527–530 http://www.jstor.org/stable/26216020 https://doi.org/10.2307/2621.60.20.

Otero-Casal, C., Patlakas, P., Prosper, M.A., Galanis, G., Miguez-Macho, G., 2019. Development of a high-resolution wind forecast system based on the WRF model and a Hybrid Kalman-Bayesian Filter. Energies 12, 3050. https://doi.org/10.3390/en12163050.

Prieto, D., Asensio, M.I., Ferragut, L., Cascón, J.M., Morillo, A., 2017. A GIS-based fire spread simulator integrating a simplified physical wildland fire model and a wind field model. Int. J. Geogr. Inf. Sci. 31, 2142–2163. https://doi.org/10.1080/13658816.2017.1334989.

Salameh, T., Drobinski, P., Vrac, M., Naveau, P., 2009. Statistical downscaling of near-surface wind over complex terrain in Southern France. Meteorog. Atmos. Phys. 103, 253–265. https://doi.org/10.1007/s00703-008-0330-7.

Sánchez, J.L., Posada, R., García-Ortega, E., López, L., Marcos, J.L., 2013. A method to improve the accuracy of continuous measuring of vertical profiles of temperature and water vapor density by means of a ground-based microwave radiometer. Atmos. Res. 122, 43–54 http://www.sciencedirect.com/science/article/pii/S016980951200350X https://doi.org/10.1016/j.atmosres.2012.10.024.

Sanz-Rodrigo, J., Chávez-Arroyo, R.A., Moriarty, P., Churchfield, M., Kosović, B., Réthoré, P.E., Hansen, K.S., Hahmann, A., Mirocha, J., Rife, D., 2017. Mesoscale to microscale wind farm flow modeling and evaluation. Wiley Interdisc. Rev. 6, e214. https://onlinelibrary.wiley.com/doi/abs/10.1002/wene.214. 10.1002/wene.214.

Skamarock, W.C., Klemp, J.B., Dudhia, J., Gill, D.O., Barker, D.M., Duda, K.G., Huang, X.Y., Wang, W., Powers, J.G., 2008. A description of the Advanced Research WRF version 3. In: Technical Note NCAR/TN-475+STR National Center for Atmospheric Research.

Solbakken, K., Birkelund, Y., 2018. Evaluation of the Weather Research and Forecasting (WRF) model with respect to wind in complex terrain. J. Phys. Conf. Ser. 1102–012011. https://doi.org/10.1088/1742-6596/1102/1/012011.

Sunyer, M., Madsen, H., Ang, P., 2012. A comparison of different regional climate models and statistical downscaling methods for extreme rainfall estimation under climate change. Atmos. Res. 103, 119–128 http://www.sciencedirect.com/science/article/pii/S016980951100189X https://doi.org/10.1016/j.atmosres.2011.06.011, Rainfall in the urban context: forecasting, risk and climate change.

Tewari, M., Chen, F., Wang, W., Dudhia, J., A.LeMone, M., Mitchell, K., Ek, M., Gayno, G., Wegiel, J., & Cuenca, R. (2004). Implementation and verification of the united NOAH land surface model in the WRF model. 20th Conference on Weather Analysis and Forecasting/16th Conference on Numerical Weather Prediction 11–15.

Tominaga, Y., Mochida, A., Okaze, T., Sato, T., Nemoto, M., Motoyoshi, H., Nakai, S., Tsutsumi, T., Otsuki, M., Uamatsu, T., Yoshino, H., 2011. Development of a system for predicting snow distribution in built-up environments: Combining a mesoscale meteorological model and a CFD model. J. Wind Eng. Ind. Aerodyn. 99, 460–468 http://www.sciencedirect.com/science/article/pii/S0167610510001376 https://doi.org/10.1016/j.jweia.2010.12.004, (The Fifth International Symposium on Computational Wind Engineering).

Trapero, L., Bech, J., Lorente, J., 2013. Numerical modelling of heavy precipitation events over Eastern Pyrenees: analysis of orographic effects. Atmos. Res. 123, 368–383 http://www.sciencedirect.com/science/article/pii/S016980951200316X https://doi.org/10.1016/j.atmosres.2012.09.014, 6th European Conference on Severe Storms 2011. Palma de Mallorca, Spain.

Verkaik, J.W., Jacobs, A.J.M., Tijm, A.B.C., Onvlee, J.R.A., 2006. Local wind speed estimation by physical downscaling of weather model forecasts. J. Wind Eng. Ind. Aerodyn.(Submitted to).

Wagenbrenner, N. S., Forthofer, J. M., Lamb, B. K., S.Shannon, K., & W.Butler, B. (2016). Downscaling surface wind predictions from numerical weather prediction models in complex terrain with Wind-

Ninja. Atmos. Chem. Phys., 16, 5229–5241. https://www.atmos-chem-phys.net/16/5229/2016/. doi: https://doi.org/10.5194/acp-16-5229-2016.

Xue, Y., Janjic, Z., Dudhia, J., Vasic, R., Sales, F.D., 2014. A review on regional dynamical downscaling in intraseasonal to seasonal simulation/prediction and major factors that affect downscaling ability. Atmos. Res. 147-148, 68–85 http://www.sciencedirect.com/science/article/pii/S0169809514002002 https://doi.org/10.1016/j.atmosres.2014.05.001.

Yamada, T., Koike, K., 2011. Downscaling mesoscale meteorological models for computational wind engineering applications. J. Wind Eng. Ind. Aerodyn. 99, 199–216 http://www.sciencedirect.com/science/article/pii/S0167610511000262 https://doi.org/10.1016/j.jweia.2011.01.024, (The Fifth International Symposium on Computational Wind Engineering).